SAND2019-7870C

Influence of Data Acquisition Algorithms on X-Ray Phase Contrast Imaging Computed Tomography

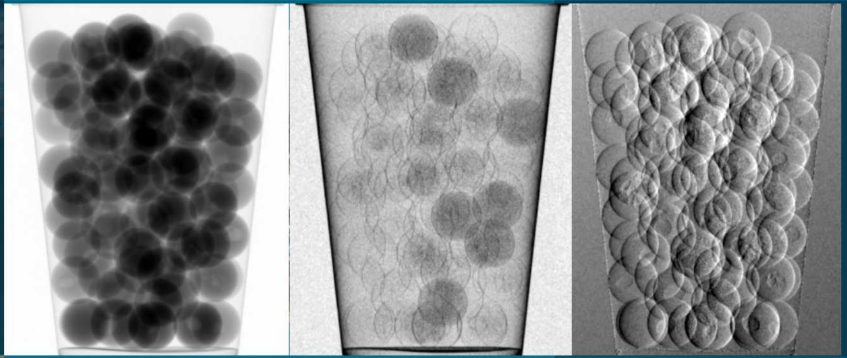

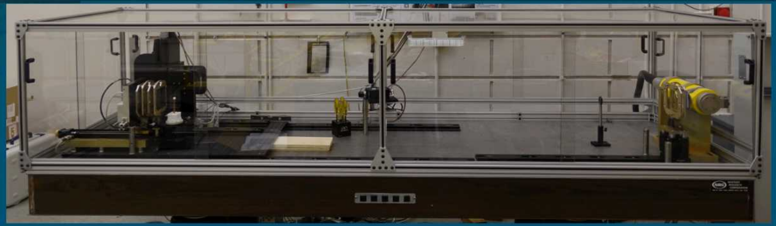

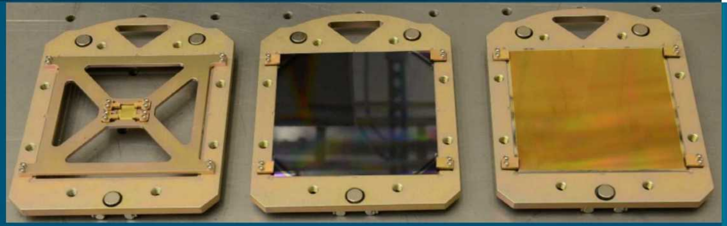

PRESENTED BY

Collin J.C. Epstein, Ryan Goodner, Kyle R, Thompson, Amber L. Dagel

QNDE 2019

2019-07-16

Sandia National Laboratories is a multimission laboratory managed and operated by National Technology & Engineering Solutions of Sandia, LLC, a wholly owned subsidiary of Honeywell International Inc., for the U.S. Department of Energy's National Nuclear Security Administration under contract DE-NA0003525.

SAND NO.

Outline

- X-ray Phase Contrast Imaging
- Acquisition Algorithms
- Data Comparison
- Conclusions

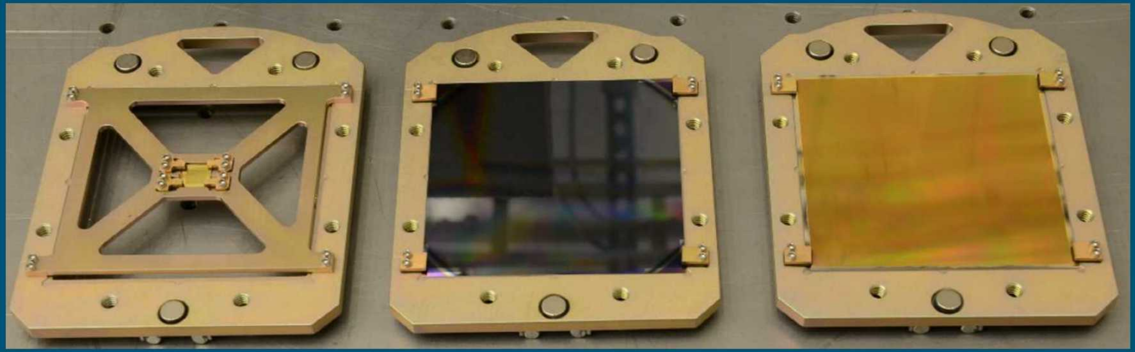

SNL large-area Talbot-Lau interferometer gratings

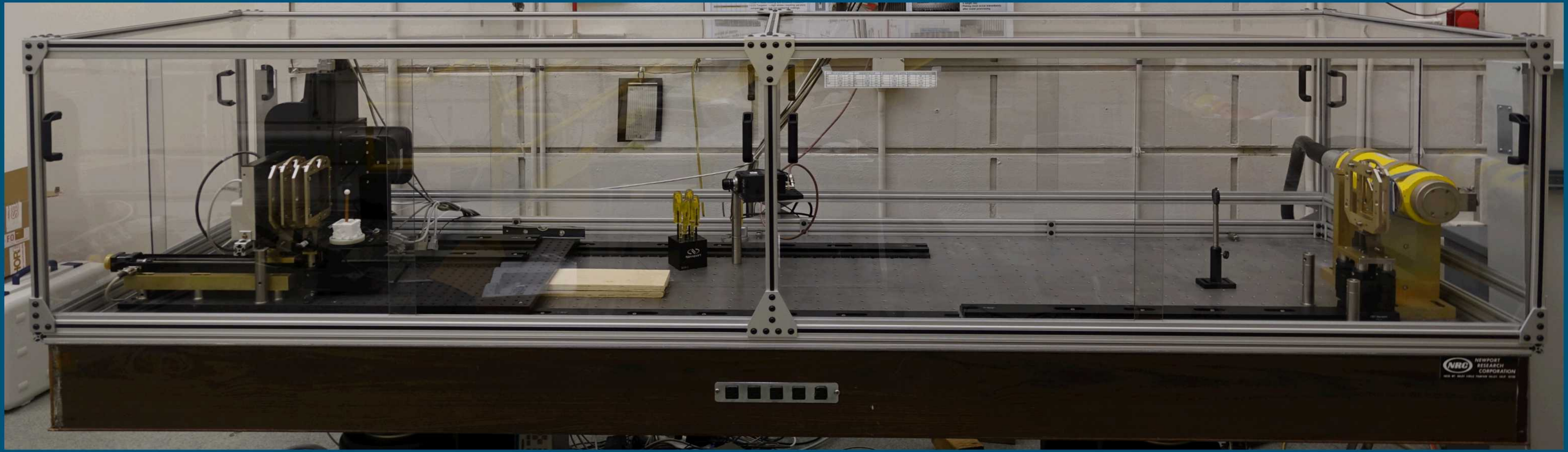

SNL Talbot-Lau XPCI System

X-Ray Phase Contrast Imaging

A brief introduction

XPCI succeeds where traditional radiography fails

Traditional radiography yields low-contrast images for low-Z components

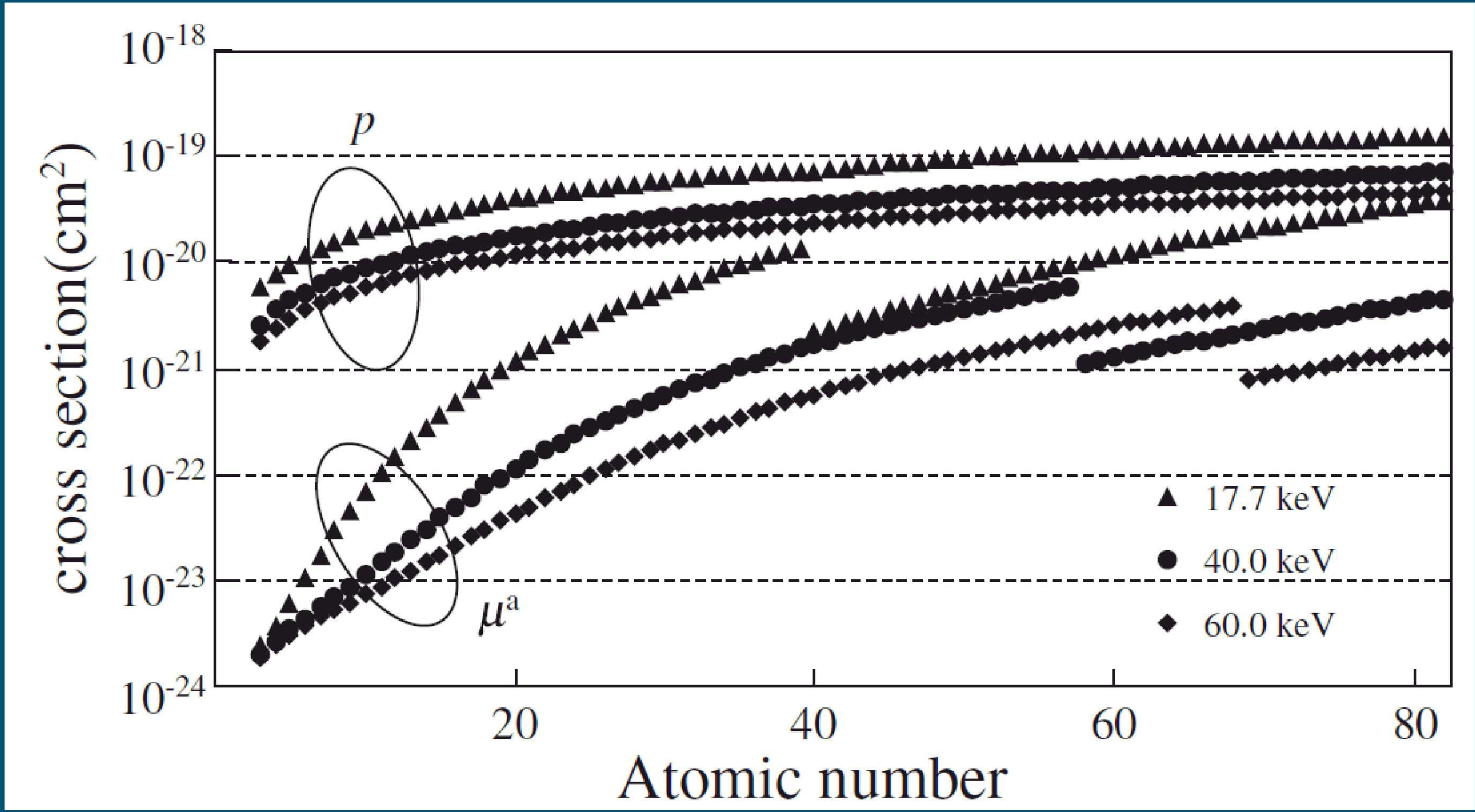

Momose, Atsushi. "Recent Advances in X-ray Phase Imaging." *Japanese Journal of Applied Physics* 44.9A (2005): 6355-367.

Our apparatus implements a Talbot-Lau Interferometer

Grating interferometer enables phase imaging using laboratory X-ray sources

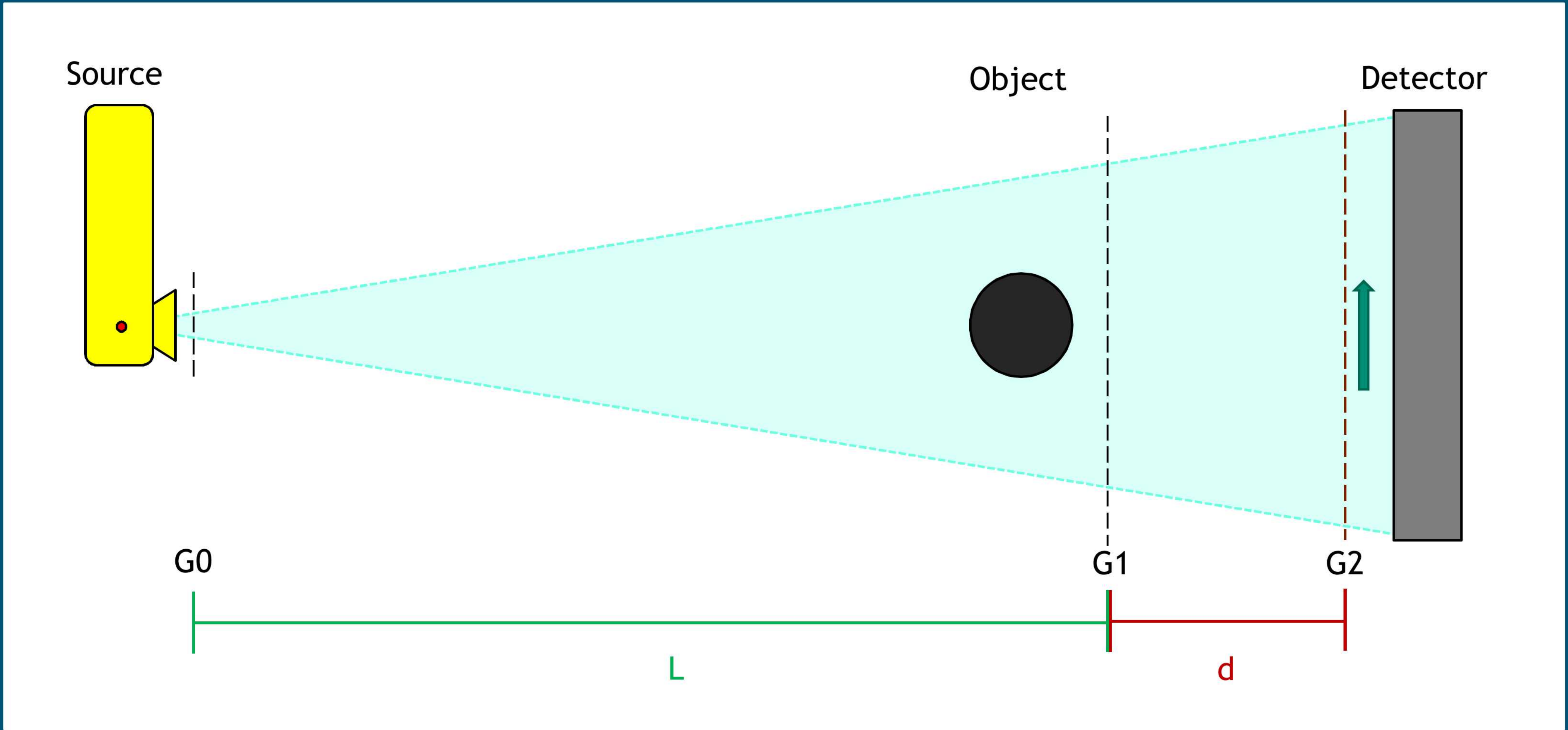

XPCI yields Trimodal Image Data

Single image set reconstructed into three distinct image products

Photograph

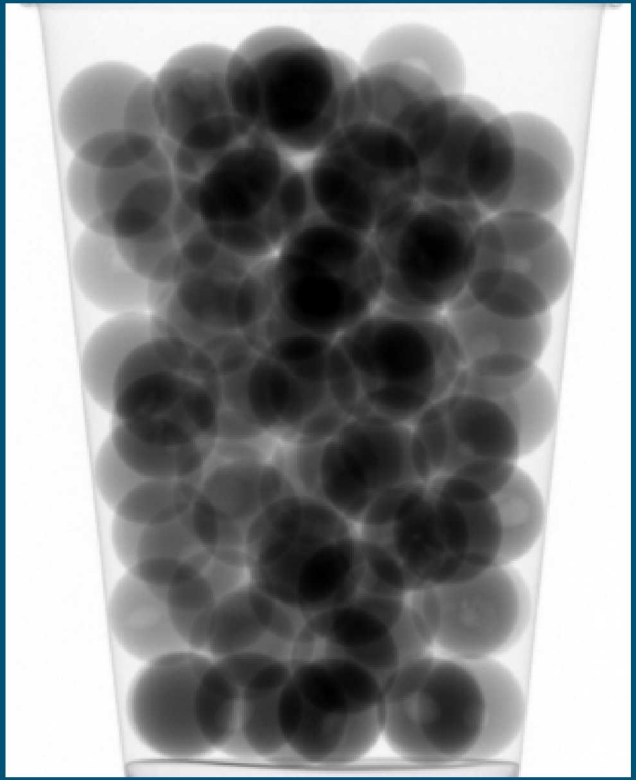

Tau

Absorption

Projection 0

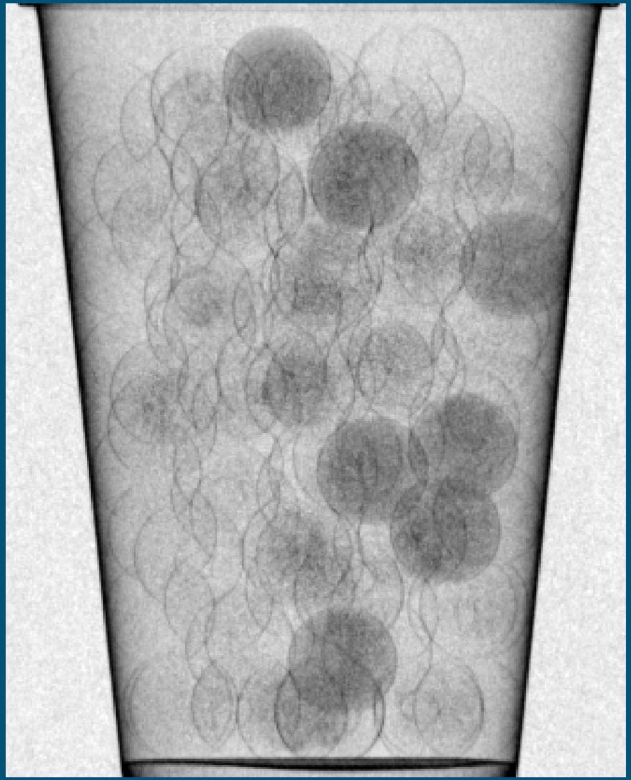

Dark Field

Small-Angle Scatter

Projection 0

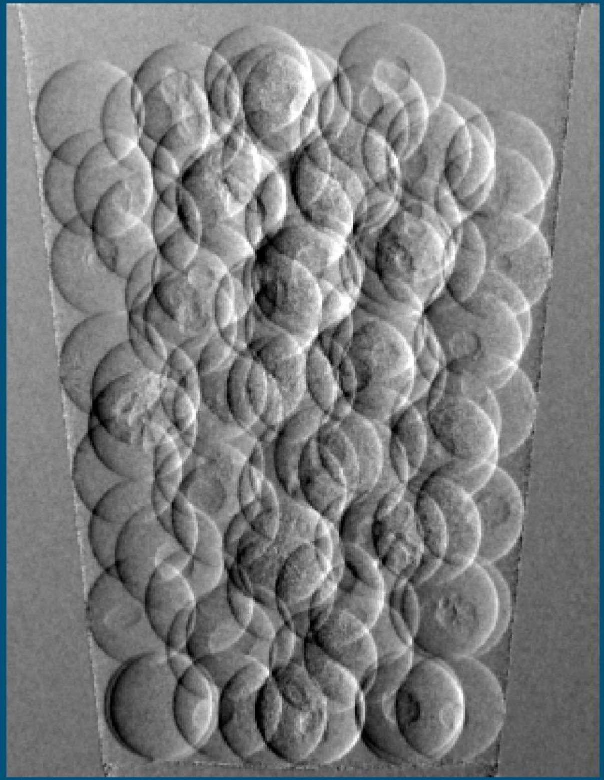

Differential Phase

Refraction

Projection 0

Acquire volumetric data using Computed Tomography

Capture data for volumetric reconstruction by rotating object

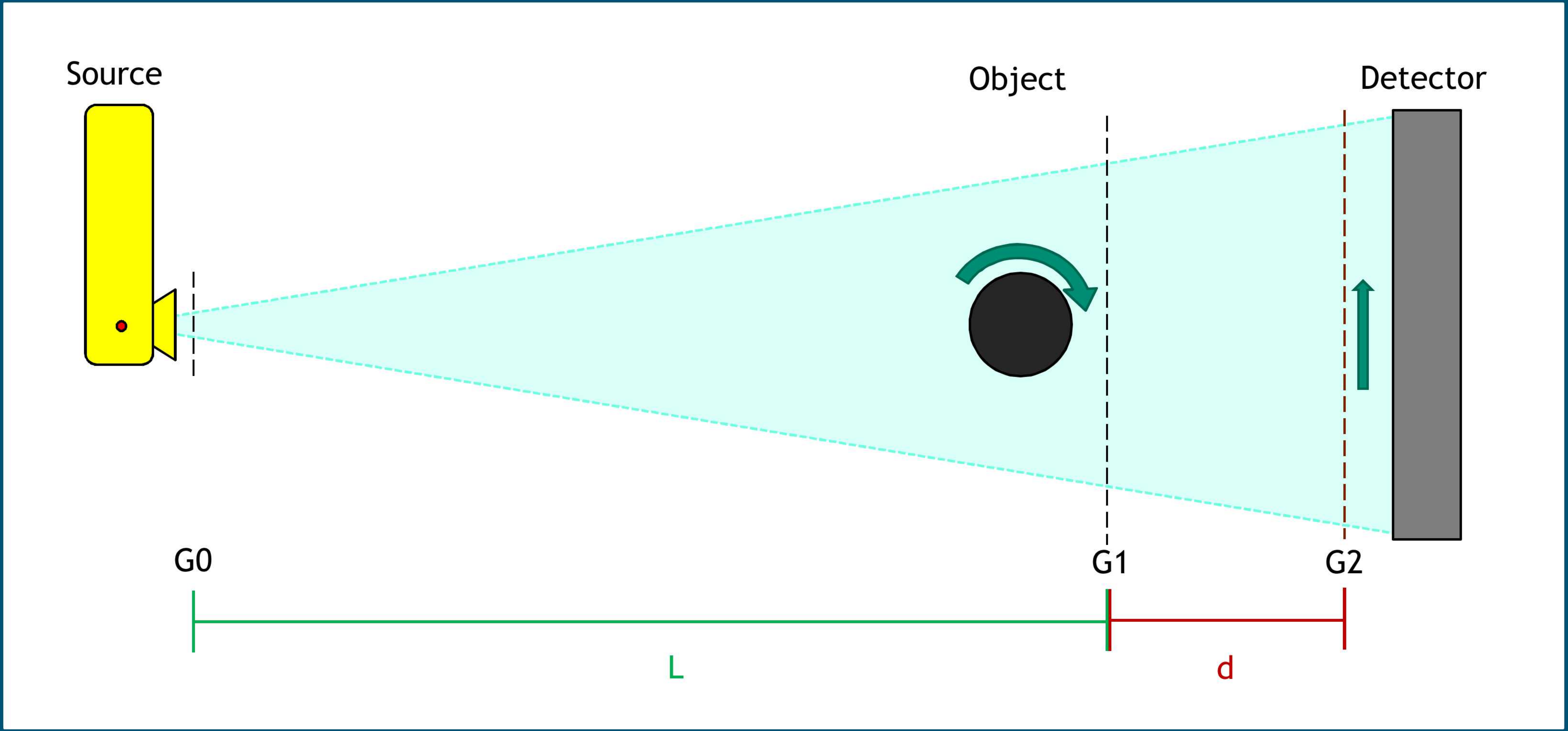

CT Reconstruction reveals object internal structure

Set of projections reconstructed to set of slices within object volume

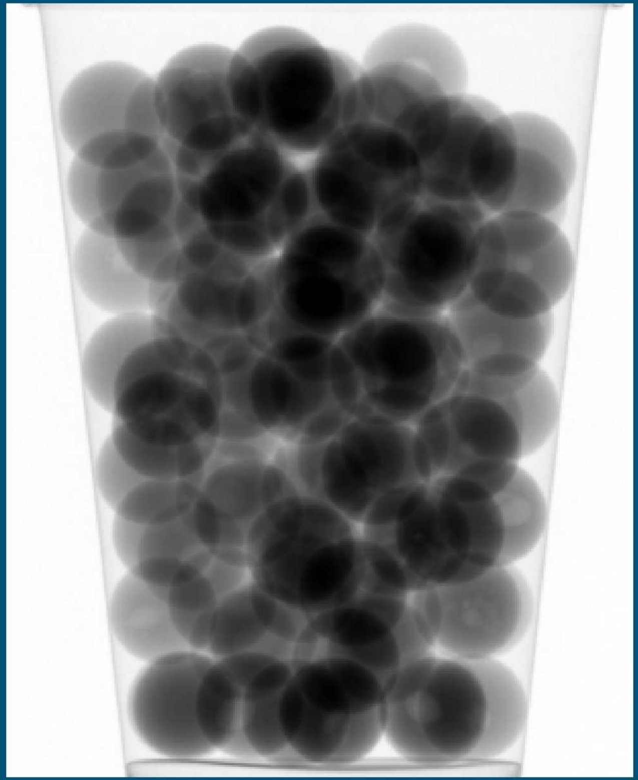

Tau

Absorption

Projection 0

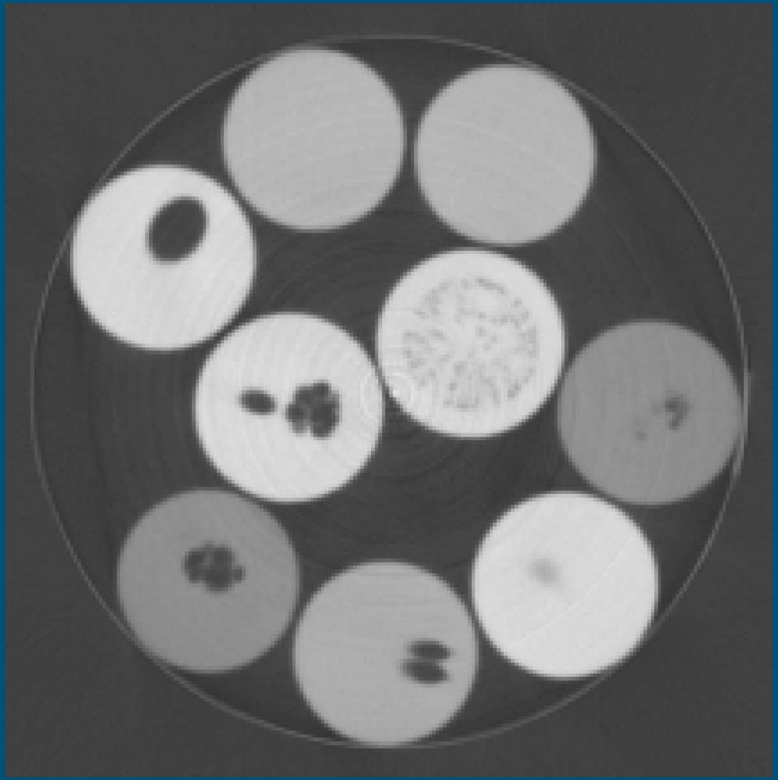

Tau

Absorption

Slice 26

Acquisition Algorithms

Different methods to acquire XPCI CT data

XPCI CT Data requires analyzer grating translation

G2 grating translation causes translation of interferometer fringes

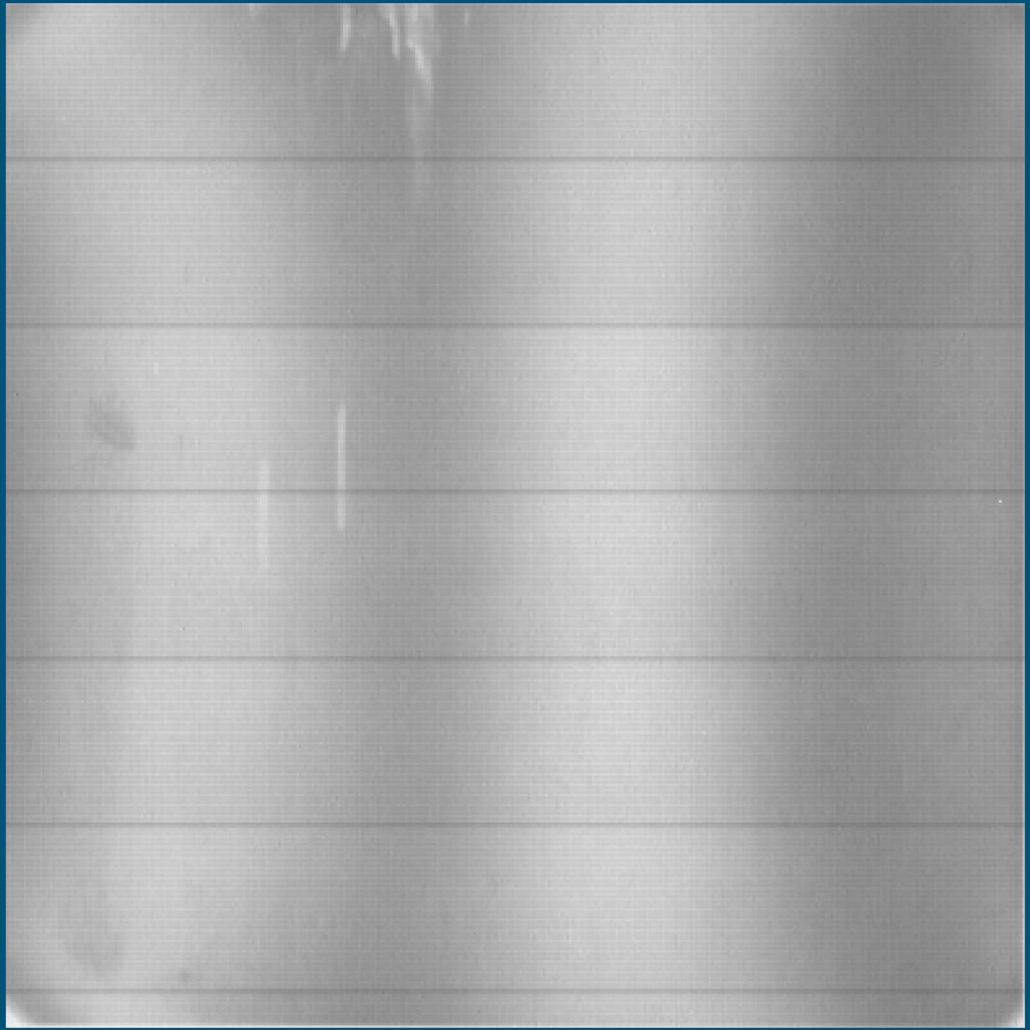

Raw reference image set (cropped)

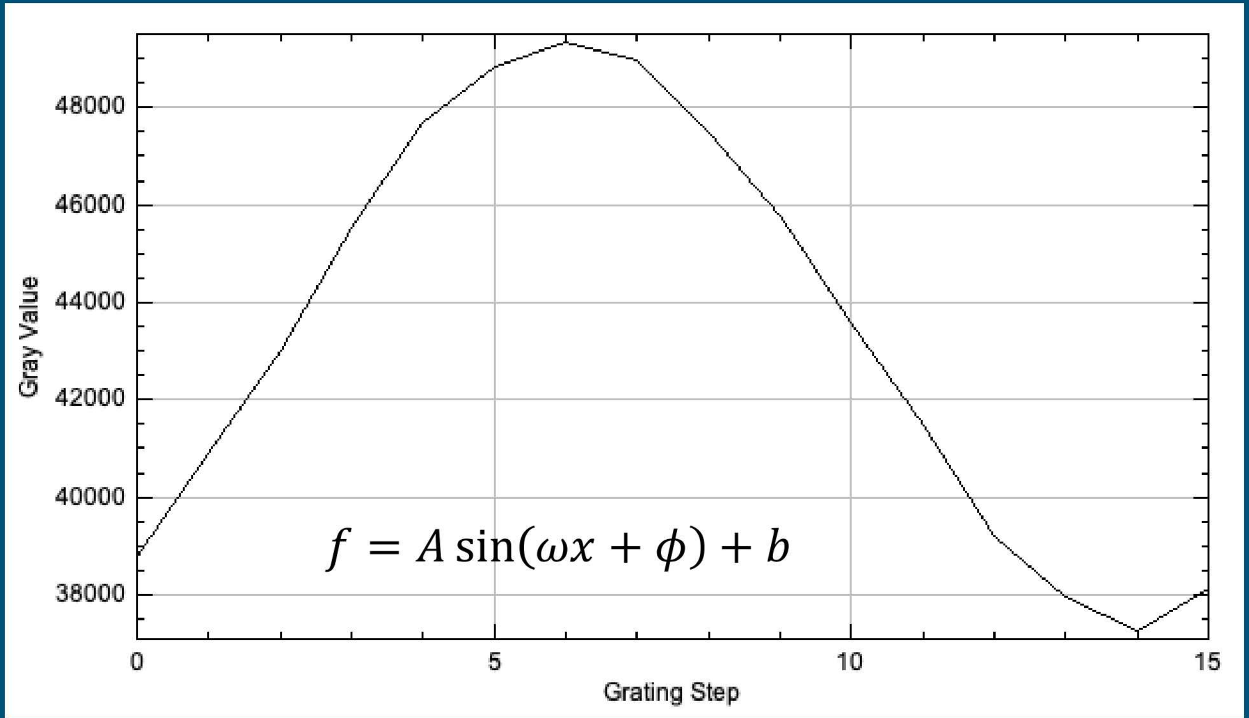

Value of pixel (158, 236)

Tau	Dark Field	Differential Phase
$\tau = \frac{b_S}{b_R}$	$DF = \frac{A_S}{A_R} \times \frac{b_R}{b_S}$	$dP = \phi_S - \phi_R$

XPCI **CT** Data requires object rotation

Number of angular projections dictated by Shannon-Nyquist Theorem

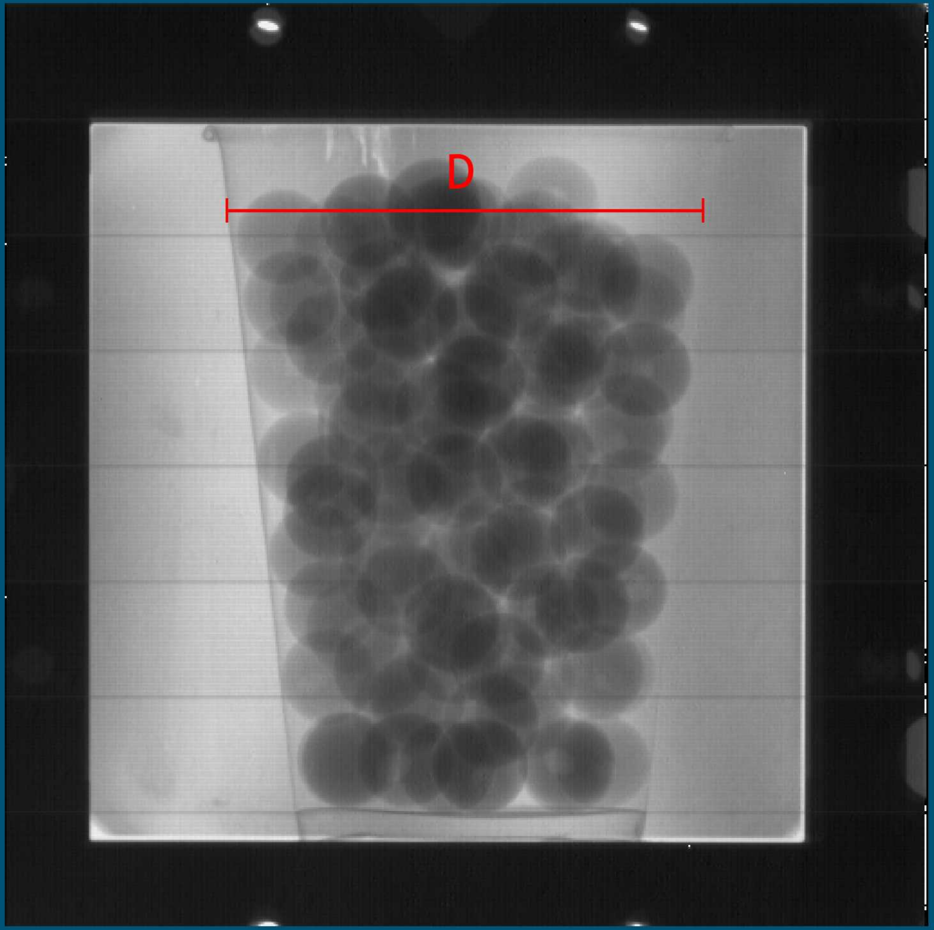

Raw sample image

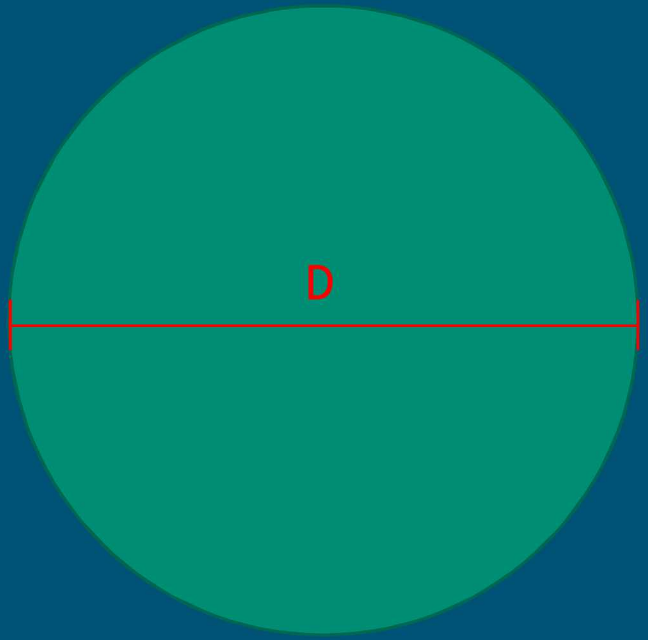

$$P \geq D * \frac{\pi}{2}$$

Step First Algorithm

Outer loop = Rotating
Inner loop = Phase stepping
Let Θ = rotational angle, x = G2 grating position

for $\boldsymbol{i} \coloneqq \mathbf{0}$ to *CT-projections* **do**

$$\boldsymbol{\theta} = \boldsymbol{\theta_0} + \Delta\boldsymbol{\theta} * \boldsymbol{i}$$

for $\boldsymbol{j} \coloneqq \mathbf{0}$ to *G2-positions* **do**

$$\boldsymbol{x} = \boldsymbol{x_0} + \Delta\boldsymbol{x} * \boldsymbol{j}$$

end

end

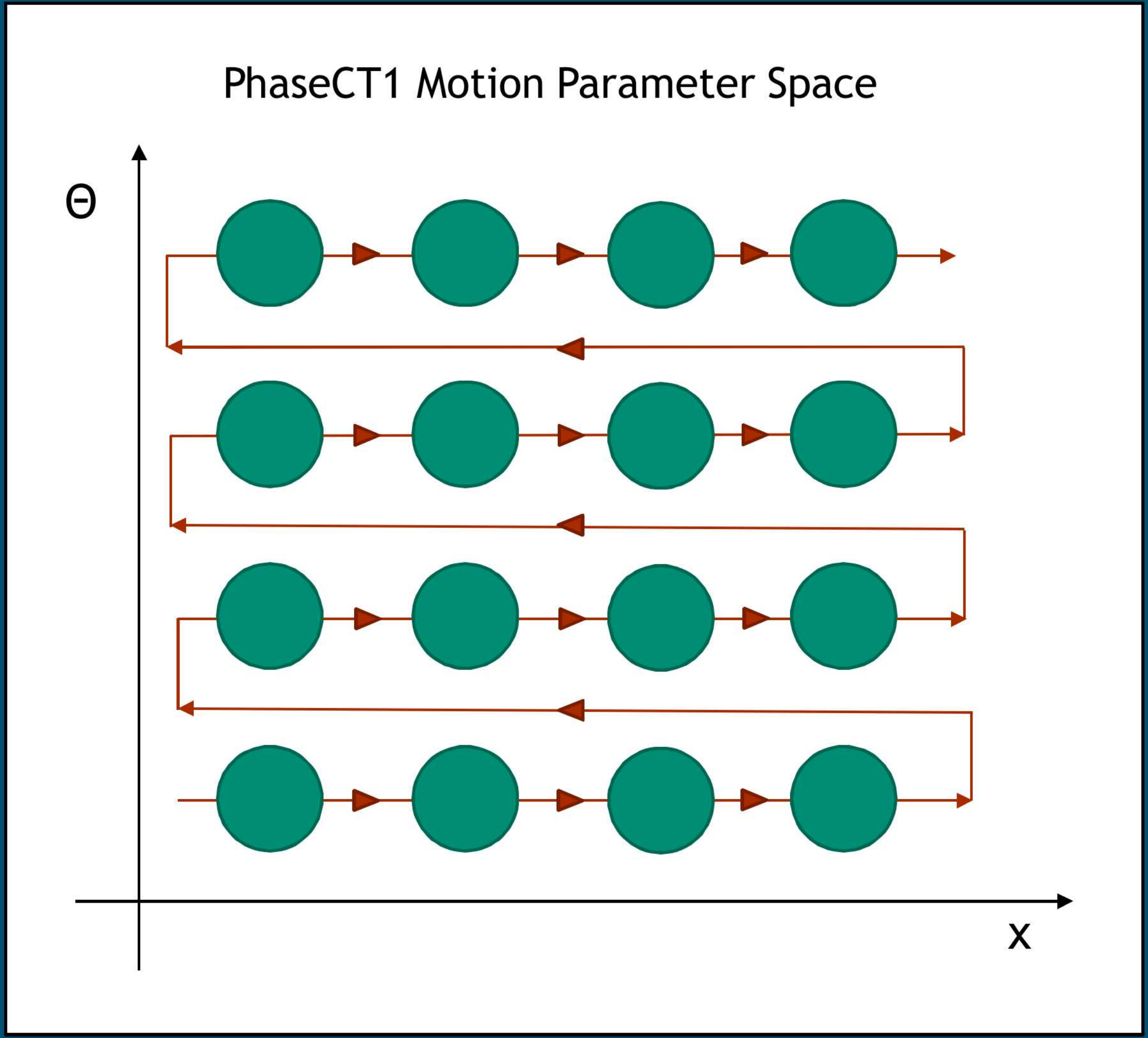

Rotate First Algorithm

Outer loop = Phase stepping
Inner loop = Rotating
Let Θ = rotational angle, x = G2 grating position

for $\boldsymbol{i} \coloneqq \mathbf{0}$ to *G2-positions* **do**
$\boldsymbol{x} = \boldsymbol{x_0} + \Delta \boldsymbol{x} * \boldsymbol{i}$
for $\boldsymbol{j} \coloneqq \mathbf{0}$ to *CT-projections* **do**
$\boldsymbol{\theta} = \boldsymbol{\theta_0} + \Delta \boldsymbol{\theta} * \boldsymbol{j}$
end
end

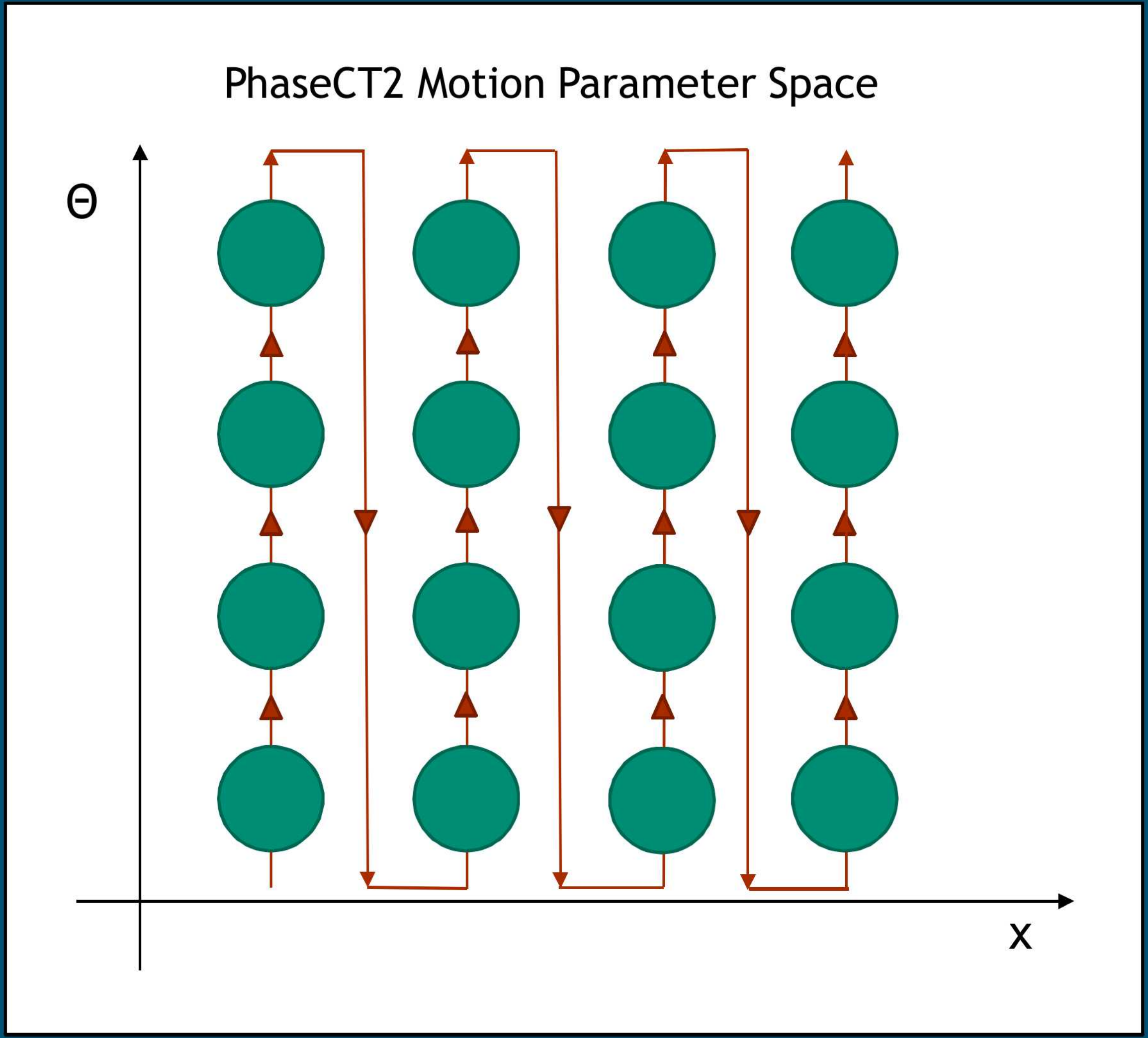

Data and Results

Comparing images acquired with the different algorithms

Fringe Motion Degradation apparent in Rotate First data

Superior fringe profile captured by Step First

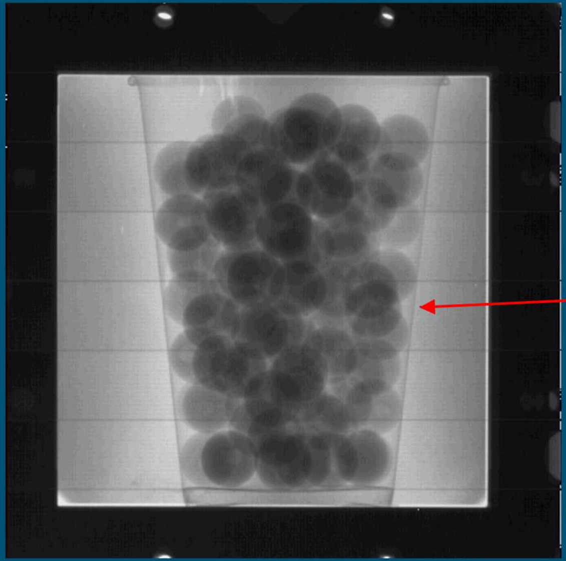

(280,130)

Raw sample image

Reference Fringe, Pixel (280,130)

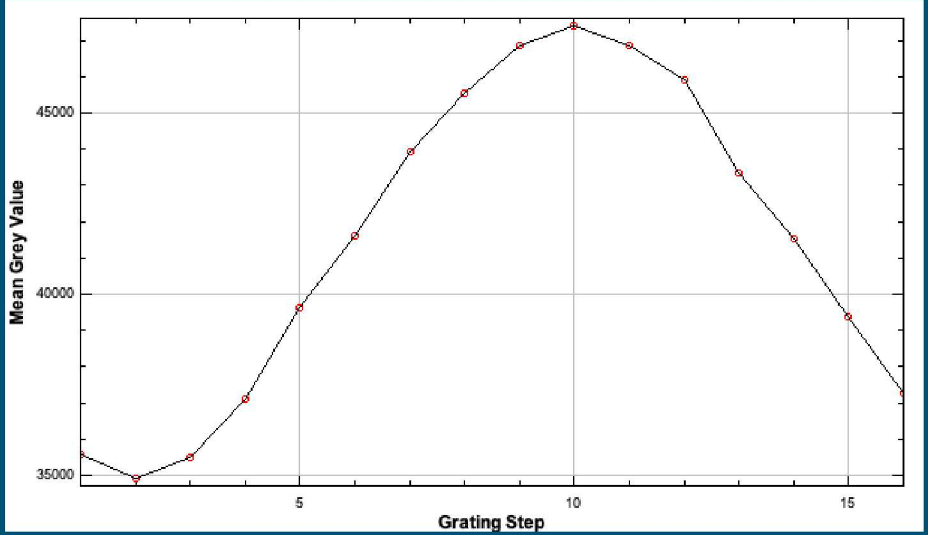

Step First Fringe, Pixel (280,130)

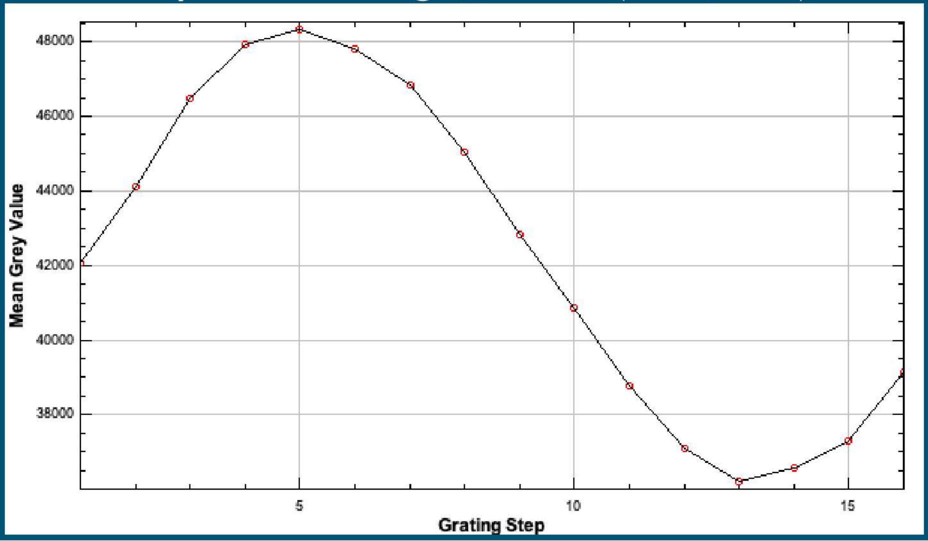

Rotate First Fringe, Pixel (280,130)

Sinogram Intensity Variation appears in Step First Data

Smoother dP sinogram ‘intensity’ profile captured by Rotate First

Step First
Differential Phase

Slice 185

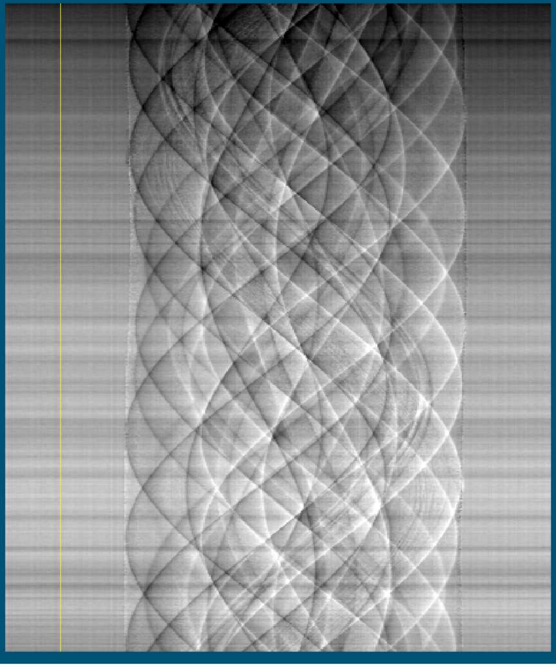

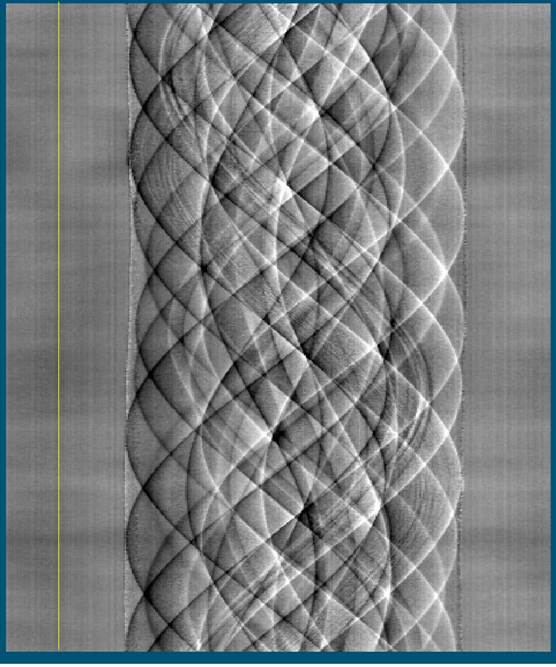

Rotate First
Differential Phase

Slice 185

Step First
Differential Phase

Slice 185
Column X=50

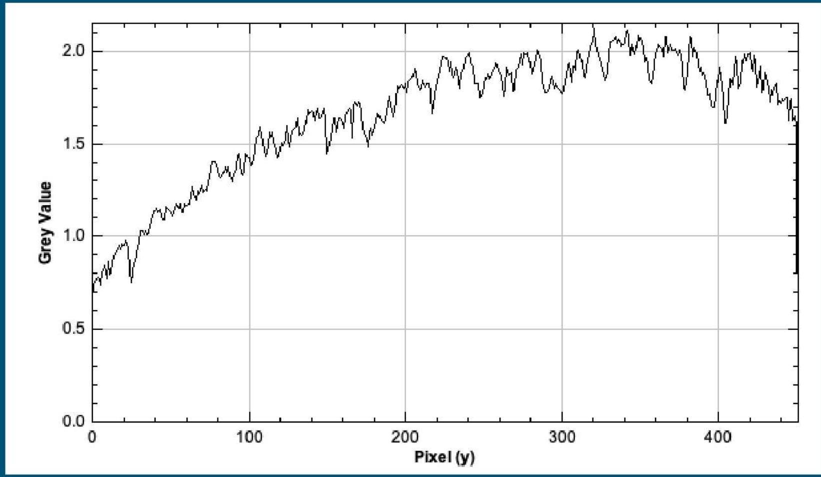

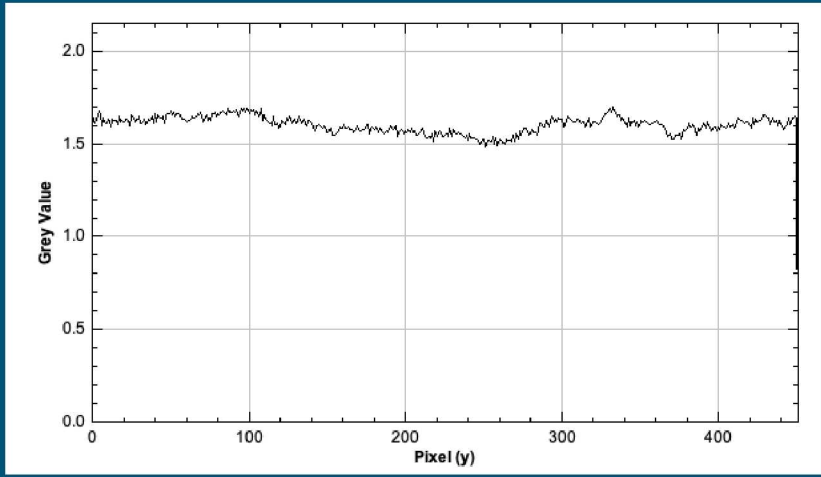

Rotate First
Differential Phase

Slice 185
Column X=50

CT Reconstructions yield similar results

Resulting CT reconstructions appear similar to the eye

Step First

Rotate First

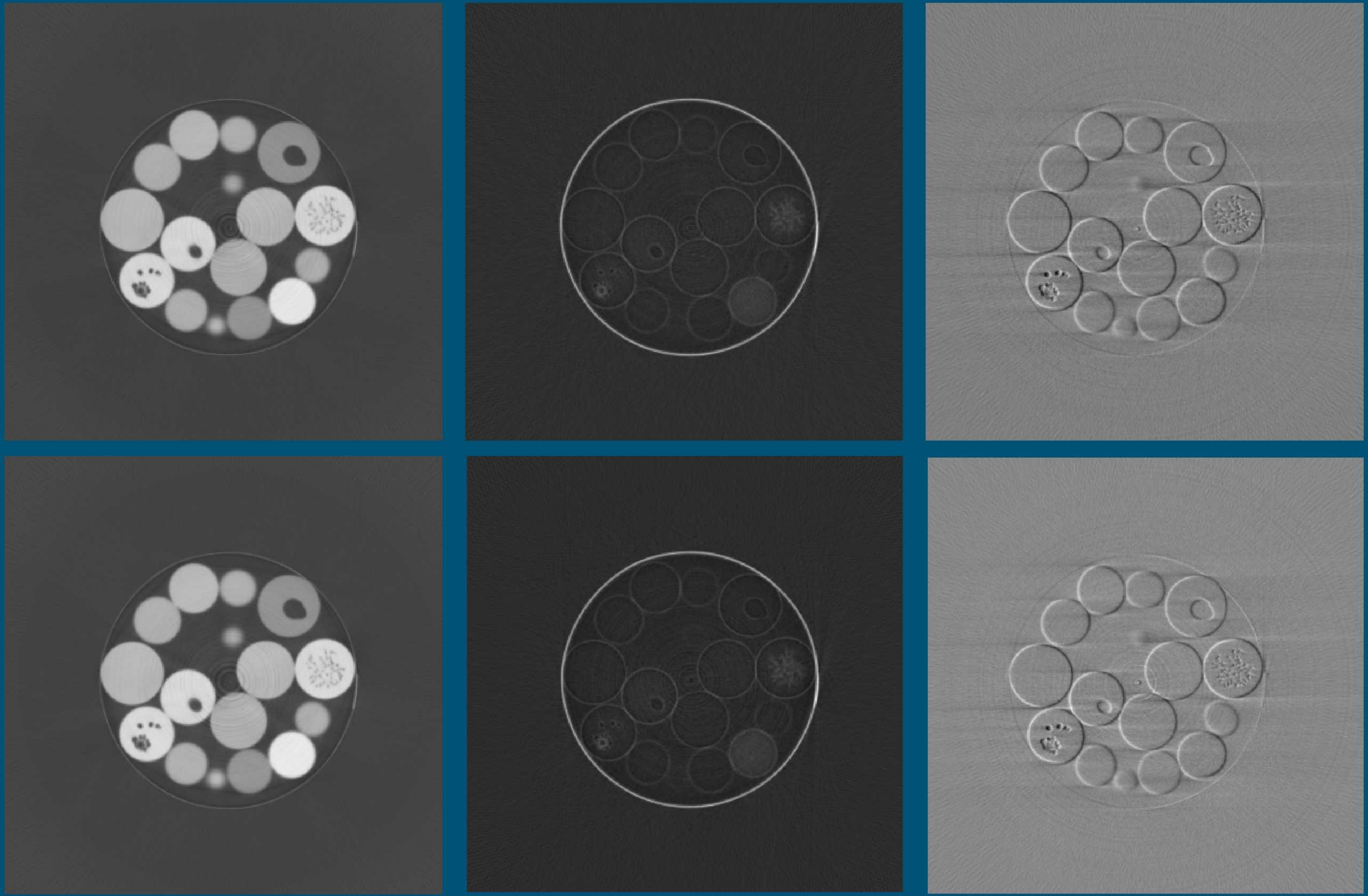

Tau

Dark Field

Differential Phase

Slice 103

CT Reconstructions do have numerical differences

Computed subtraction between slices reveals minute but distinct differences

Result of (Step First data) – (Rotate First data)

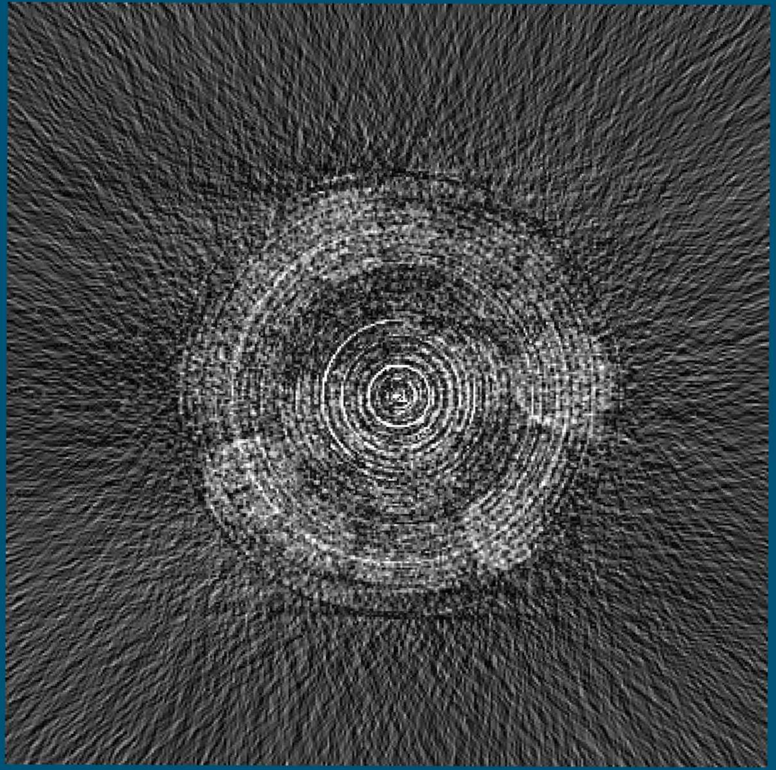

Tau

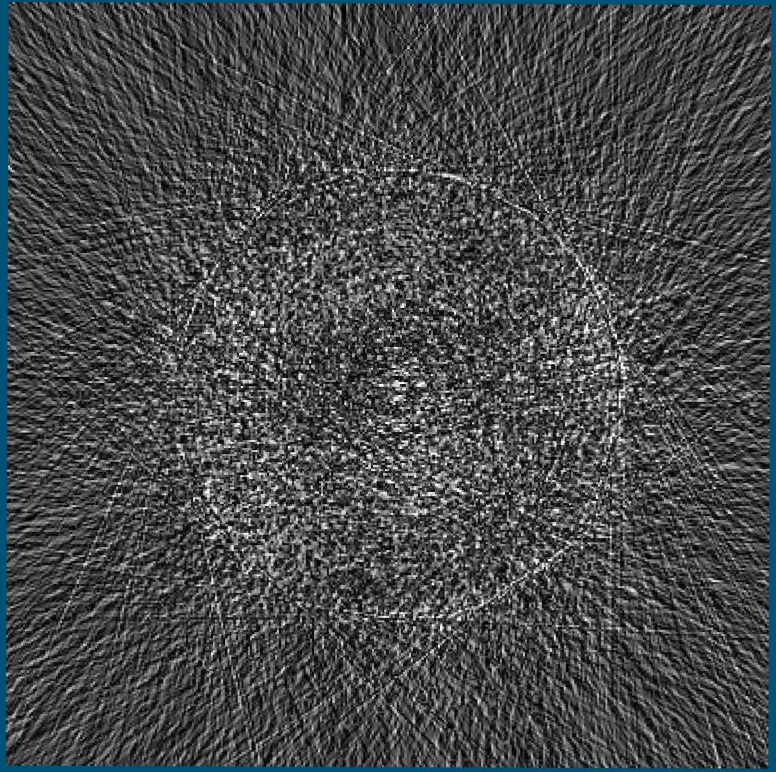

Dark Field

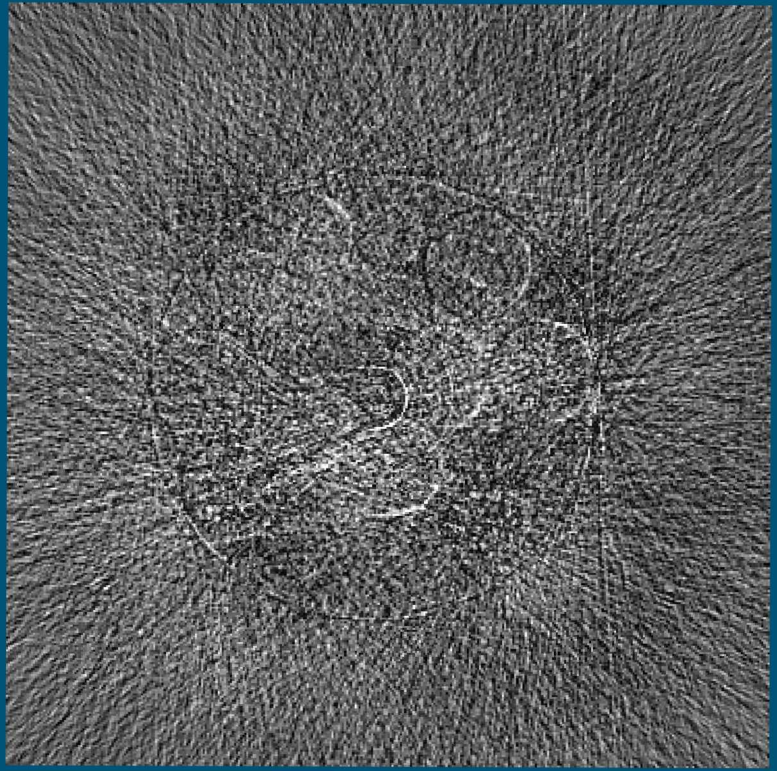

Differential Phase

Slice 103

Conclusions

Choosing an algorithm

Conclusions

- Use PhaseCT1 as primary acquisition algorithm
  - Superior fringe profile yields more accurate XPCI reconstruction
  - Intensity variations easily normalized for CT reconstruction
  - In case of failure, yields partial dataset that can be reconstructed
- Con: ineligible for continuous scan (slower)
- Hypothesis: system error largely due to thermal drift

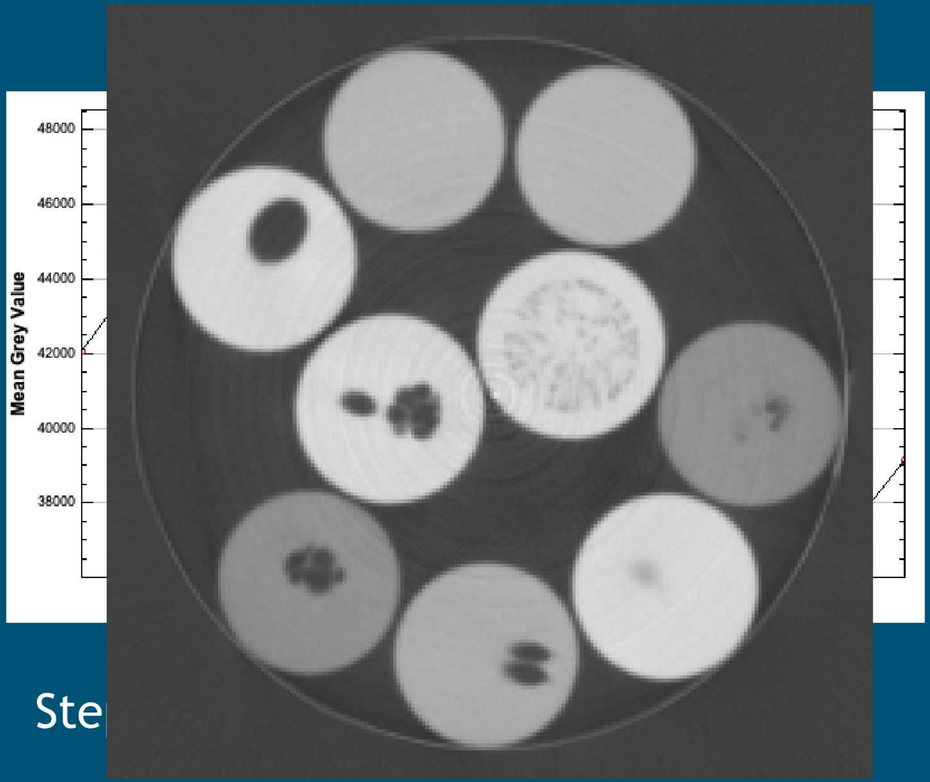

Ste

Tau

Acknowledgements

Thanks to Ryan Goodner, Kyle R. Thompson, and Amber L. Dagel and the rest of the SNL XPCI Encapsulants/Rapid3D teams.

This paper describes objective technical results and analysis. Any subjective views or opinions that might be expressed in the paper do not necessarily represent the views of the U.S. Department of Energy or the United States Government.

This work was supported by the Laboratory Directed Research and Development program at Sandia National Laboratories.

References

- Momose, Atsushi. "Recent Advances in X-ray Phase Imaging." *Japanese Journal of Applied Physics* 44.9A (2005): 6355-367.
- Pfeiffer, F., et al. "Tomographic reconstruction of three-dimensional objects from hard X-ray differential phase contrast projection images." *Nuclear Instruments and Methods in Physics Research Section A: Accelerators, Spectrometers, Detectors and Associated Equipment* 580.2 (2007): 925-928.
- Pfeiffer, Franz, et al. "Phase retrieval and differential phase-contrast imaging with low-brilliance X-ray sources." *Nature physics* 2.4 (2006): 258.
- Pfeiffer, F., et al. "Hard x-ray phase tomography with low-brilliance sources." *Physical review letters* 98.10 (2007): 108105.
- Zanette, I., et al. "Interlaced phase stepping in phase-contrast x-ray tomography." *Applied Physics Letters* 98.9 (2011): 094101.
- Zanette, I., et al. "Trimodal low-dose X-ray tomography." *Proceedings of the National Academy of Sciences* 109.26 (2012): 10199-10204.
- Fu, Jian, et al. "Helical differential X-ray phase-contrast computed tomography." *Physica Medica* 30.3 (2014): 374-379.
- Bevins, Nicholas, et al. "Multicontrast x-ray computed tomography imaging using Talbot-Lau interferometry without phase stepping." *Medical physics* 39.1 (2012): 424-428.
- Kharfi, Faycal. "Mathematics and Physics of Computed Tomography (CT): Demonstrations and Practical Examples." *Imaging and Radioanalytical Techniques in Interdisciplinary Research-Fundamentals and Cutting Edge Applications*. IntechOpen, 2013.
- Dagel, Amber L., et al. "Optimization of hardware and image processing for improved image quality in x-ray phase contrast imaging." *Anomaly Detection and Imaging with X-Rays (ADIX) IV*. Vol. 10999. International Society for Optics and Photonics, 2019.